Optical Materials 85 (2018) 356–362

Contents lists available at ScienceDirect

Optical Materials

journal homepage: www.elsevier.com/locate/optmat

Mapping lattice-induced plasmon modes in metallic nanoantenna arrays using fluorescence decay of semiconductor quantum dot bioconjugates

Seyed M. Sadeghi[a,b,*], Rithvik R. Gutha[a,b], Christina Sharp[a], Ali Hatef[c]

[a] Department of Physics and Astronomy, University of Alabama in Huntsville, Huntsville, AL, 35899, USA
[b] Nano and Micro Device Center, University of Alabama in Huntsville, Huntsville, AL, 35899, USA
[c] Department of Computer Science and Mathematics, Nipissing Computational Physics Laboratory (NCPL), Nipissing University, North Bay, ON, P1B 8L7, Canada

ARTICLE INFO

Keywords:
Plasmonic coupling
Surface lattice resonances
Nanorods
Localized surface plasmon resonances
Refractive index sensitivity
Extinction
Gold nanoantennas

ABSTRACT

We use the fluorescence decay of quantum dot bioconjugates and their size distribution as near field probes to investigate lattice-induced plasmonic resonances and their interaction with excitons. The quantum dots are biologically immobilized on gold nanoantenna arrays while their spontaneous emission decay rates are spectrally resolved. Our results show that the periodic arrangement of the nanoantennas can generate or optically activate certain plasmonic resonances, different from their intrinsic plasmon modes. This includes formation of a hybrid photonic-plasmonic dipole mode that can strongly couple with the quantum dots, making their decay rates anisotropic and wavelength dependent. The anisotropic decay is decided by the shapes and sizes of the nanoantennas and by the direction of the quantum dot dipoles. The results suggest lattice-induced plasmonic resonances can be used as engineered states to drive transfer of energy between quantum dots at certain wavelengths.

1. Introduction

Metallic nanoantennas (mANTs) can be used for detection of biological molecules [1], enhancement of Forster resonance energy transfer (FRET) between semiconductor quantum dots (QDs) [2], emission enhancement of QDs, formation of exciton-plasmon coupling [3,4], etc. Recent reports have shown the impact of localized surface plasmon resonances (LSPRs) of mANTs on QDs can be controlled by placing them in the vicinity of Si/Al oxide junctions [5]. Such junctions can suppress the defect environment of the QDs, making them superbright [6,7]. The impact of mANTs can also be enhanced by arranging them in the form of periodic arrays. Such arrays can support surface lattice resonances (SLRs) that can be weakly or strongly coupled with excitons [8–10]. SLRs are formed via hybridization of LSPRs and photonic modes of the arrays [11]. Additionally, when mANTs are very close to each other they can support certain states via redistribution of charges. For the case of dimers, for example, as their spacing decreases the dominant dipole of mANTs is red shifted until new states are formed. This is associated with a large pileup of induced charges in the gaps and capacitive coupling between plasmon modes [12].

In the case of periodic arrays of mANTs, SLRs occur when the LSPR wavelengths are close to those of the Rayleigh Anomaly (RA), allowing light diffraction to happen in the plane of the mANTs. In addition to such extended modes, depending on the wavelength, such arrays can also support periodic localized photonic modes. Instead of collective interaction with the whole array, as in the case of SLRs, these modes interact with individual mANTs locally, forming hybrid photonic-plasmonic states or lattice-induced plasmonic modes (LIPMs). In a recent report we showed that such hybrid modes can support ultrahigh refractive index sensitivity of 925 nm/RIU (refraction index unit), far higher than those reported for the intrinsic LSPRs modes of mANTs [13]. The objective of this paper is to use decay dynamics of QDs as a probe to investigate near fields of LIPMs. For this we use QDs that are tagged with streptavidin (s-QDs) and are biologically conjugated to mANTs, covering them closely (Fig. 1a). We investigate interaction between excitons in such QDs with LIPMs. Considering the size distribution of such QDs, this allows us to map the dynamics of excitons as a function of wavelength (Fig. 1b). We show that for given sizes and shapes of mANTs, their periodic arrangement can support a dipole-like LIPM. Such a mode can interact efficiently with s-QDs at certain energies and QD dipole alignment. This leads to efficient QD-LIPM energy transfer (Intra-F), promoting inter-dot Forster resonance energy transfer (Int-F) from smaller QDs to the larger ones (Fig. 1b). These results show that LIPMs can be used to engineer plasmonic states of mANTs and their interaction with QDs.

* Corresponding author. Department of Physics and Astronomy, University of Alabama in Huntsville, Huntsville, AL, 35899, USA.
E-mail address: seyed.sadeghi@uah.edu (S.M. Sadeghi).

https://doi.org/10.1016/j.optmat.2018.08.069
Received 5 July 2018; Received in revised form 27 August 2018; Accepted 29 August 2018

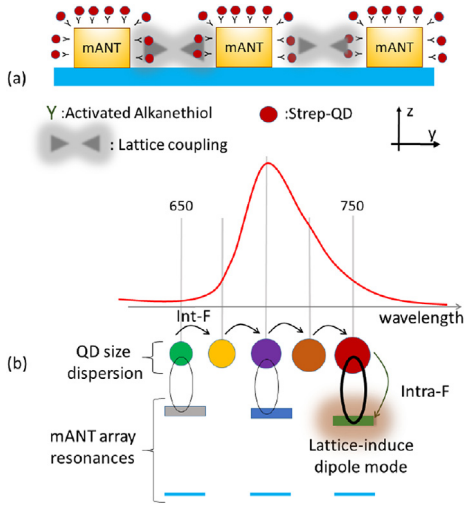

Fig. 1. Schematic of biological coating of an array of mANTs with s-QDs (a) and inter-dot (Int-F) and QD-LIPM energy transfer (Intra-F) (b) in the presence of LIPMs. The red line in (b) refers to the emission spectrum of s-QDs. Filled circles refer to the size distribution of the monodispersed s-QDs. (For interpretation of the references to color in this figure legend, the reader is referred to the Web version of this article.)

2. Methodology

We used e-beam lithography to fabricate two types of mANTs on glass substrates (Fig. 2a and a′ insets). The lengths and widths of these mANTs were ~320 and ~250 nm (sample A), and ~800 and ~150 nm (sample B). Their lattice constants along y-axis were 0.5 μm, but along the x-axis they were 0.5 μm for samples A and 1 μm for sample B. The nominal thickness of the mANTs was 40 nm. To measure extinction spectra of these samples we used a transmission setup consisting of a halogen lamp, polarizer, microscope objective, and collective lens. Samples were placed between the objective and the collective lens

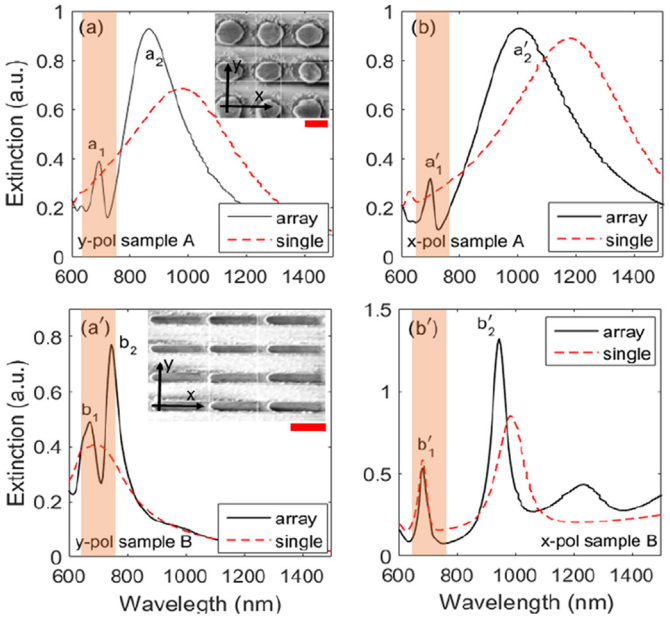

Fig. 2. Simulation results for samples A ((a) and (b)) and B ((a′) and (b′)) when the incident light is polarized along the y-axis (a) and x-axis (b). The dashed lines refer to the corresponding spectra of single mANTs in each sample. The insets in (a) and (a′) show the SEM images of samples A and B, respectively. The scale bar in (a) is 300 nm and in (a′) is 600 nm. The highlighted regions is QDs' 650–750 nm emission span.

which directed part of the transmitted light towards a wide range (400–1650 nm) sensitive spectrometer. We put a polarization analyzer before the collective lens. The decays of s-QDs were measured using a time correlated single photon counter system when the axis of this analyzer was either x- or y-axis (Fig. 2 insets). In the following we refer to such decays as x-p and y-p, respectively. A monochromator was used before the detector of the photon counter to disperse the s-QD emission at different wavelengths. For immobilization of s-QDs onto the mANT arrays, we used a carboxylic terminated self-assembled monolayer (SAM). Then this was followed by conjugation of such arrays with s-QDs [14]. The QDs were acquired from ThermoFisher [15]. They were consisted of CdSeTe cores with ZnS shells with 5–10 covalently bonded streptavidin molecules. Judging by the wavelengths of their emission, the average core size of these QDs was about 3 nm [16].

To study the mode profiles of the arrays in this paper we used COMSOL MultiPhysics. For this we considered the mANTs had small curvatures with radius (3 nm) on the top corners. We applied a two dimensional free triangular mesh on the surface of the gold and on the interfaces, using the Comsol-defined “extremely fine” size. A two-dimensional free triangular mesh was also applied to the sides of the geometry. A three-dimensional free tetrahedral mesh was used for the rest of the geometry. The minimum mesh size was considered to be 1.6 nm.

3. Lattice-induced plasmonic modes

We start our investigation considering the simulation results for samples A and B. For the case of sample A, when the incident light is polarized along the y-axis (y-pol), we expect to see two peaks, a_1 and a_2 (Fig. 2a, solid line). When the incident light is polarized along the x-axis (x-pol), the spectrum also supports two peaks, a'_1 and a'_2 (Fig. 2b, solid line). The spectral width of a'_2, however, is much wider than that of peak a_2. For the case of sample B (Fig. 2a′ and 2b′), however, the optical spectra are much narrower. Here for y-pol we see two main peaks close to each other (b_1 and b_2). For x-pol, as seen in Fig. 2b′, there is a sharp peak at 685 (b'_1) and another one at 945 (b'_2). The dashed lines in these figures show the results of simulations for single mANTs, indicating very different optical responses than those of the arrays. It seems, in particular, that the most prominent effect of the arrays belongs to the case of sample B for y-pol (Fig. 2a′).

The regions highlighted in Fig. 2 show the spectral emission range of the s-QDs, from 650 nm to 750 nm. As depicted in Fig. 1b, this range refers to the shortest and longest wavelength limits of the emission spectrum of the s-QDs (red solid line). As highlighted in Fig. 1b and 650 nm corresponds to the smallest and 750 nm to the largest cores of the s-QDs in their size distribution. To obtain a better picture of how the modes of the mANT arrays in samples A and B influence exciton dynamics, in Figs. 3 and 4 we show the modal field enhancement profiles associated with the main spectral features seen in Fig. 2. These profiles are the ratios of the fields in the presence to those in the absence of the mANT arrays. The wavelengths that match the s-QDs spectral widths are highlighted with three colored filled circles, indicating the smallest, medium, and largest core sizes of the s-QDs. Note that the x-y plane is located at the interface between the mANTs and the glass substrates, while the z-y plane passes through the middle of mANTs.

For the case of sample A for y-pol (Fig. 3a), at 650 nm we mostly see the weak edge fields (panel 1). Additionally, based on the results for z-y plane in this panel, the photonic fields at this wavelength in the superstrate are nearly uniform but in the substrate were more localized. Similar situation is repeated for the x-pol (Fig. 3b, panel 1). For y-pol at 695 nm (peak a_1) and for x-pol at 700 nm (peak a'_1) the edge modes remain similar, while the photonic modes in the substrate becomes intensified (panels 2 in Fig. 3a and b). With further increase of wavelength the photonic modes are moving towards the mANTs. At 750 nm, as seen in Fig. 3a (panel 3), this leads to photonic-plasmonic coupling. This also happens for x-pol, but to a much lesser extent (Fig. 3b, panel